Version July 8, 2002

Exchange energy representations in computational micromagnetics

M. J. Donahue and R. D. McMichael

National Institute of Standards and Technology, Gaithersburg, MD, USA

In order to solve Brown's equations, which describe a continuous medium, computational micromagnetic modeling requires a discrete representation of the magnetization $\mathbf{M}(\mathbf{r})$, and a discrete representation of the derivatives of $\mathbf{M}(\mathbf{r})$ must be chosen. This choice may be made through an explicit choice of interpolation or through the choice of numerical representation of Brown's equations. In this paper we describe some alternative representations of the exchange energy on a square 2-D grid, and test these representations though comparison with analytical results for magnetization spirals and with simulations testing vortex and domain wall mobility.

Keywords: Micromagnetics, Exchange, Hysteresis

Correspondence to:
R. D. McMichael
Rm B152, Bldg 223
NIST
Gaithersburg, MD 20899
Tel: (301) 975-5121
Fax: (301) 975-4553
Email: rmcmichael@nist.gov

The field of computational micromagnetics has been growing rapidly in recent years as magnetic imaging techniques have achieved higher resolution, and devices of interest have decreased in size. Despite the fact that powerful computational resources have also become less expensive, many micromagnetic calculations of continuous thin films are carried out with a discretization that is too coarse to accurately represent the magnetization everywhere [1, 2, 3]. Indications of too coarse grids in thin film modeling include Néel walls with oppositely directed magnetization on neighboring nodes and vortices without out-of-plane vortex cores. In many cases of interest, the magnetic element being modeled is several orders of magnitude larger than the typical dimension of such a feature, so accurate calculation of these features requires a very large number of nodes and a correspondingly large amount of computational time and memory.

In this paper we demonstrate the features of a number of discrete representations of the exchange energy in micromagnetic calculations with the goal of identifying and minimizing the effects of using a grid with a spacing that is coarser than the size of the smallest micromagnetic features. For the purposes of this paper, we restrict ourselves to a rectangular grid. In the continuum representation, the exchange energy density, E_{ex}, is given by

$$E_{\mathrm{ex}} = A \int_V (\nabla m_x)^2 + (\nabla m_y)^2 + (\nabla m_z)^2 \, dV, \tag{1}$$

where m_x, m_y, and m_z are the Cartesian components of $\mathbf{m} = \mathbf{M}/|M|$. For the discrete magnetization $\mathbf{M}_i$, defined at grid points i, there are a number of choices for the representation of (1) that, in at least some cases, correspond to a particular choice of interpolation of the magnetization between grid points. The effective field acting on moment $\mathbf{M}_i$ is given by $\mu_0 \mathbf{H}_{\mathrm{ex},i} = -dE_{\mathrm{ex}}/d\mathbf{M}_i$.

1 Exchange Representations

1.1 Four-neighbor dot product

The most commonly reported representation for the exchange energy on a rectangular grid is a four neighbor dot product [4, 5, 6, 7, 8, 9]:

$$E_{\mathrm{ex,4dot}} = A \sum_i \sum_{nn=1}^{4} (1 - \mathbf{m}_i \cdot \mathbf{m}_{nn}). \tag{2}$$

(The inner sum is over the 4 nearest neighbors of node i.) Using this representation of the exchange energy, the exchange field at node i is given by

$$\mathbf{H}_{\mathrm{ex,4dot},i} = \frac{2A}{\mu_0 M} \sum_{nn=1}^{4} \mathbf{m}_{nn}. \tag{3}$$

One shortcoming of this representation is that it does not accurately represent the torque when the angle between neighboring moments is large. To illustrate this, consider two neighboring moments, $\mathbf{m}_i$ and $\mathbf{m}_j$. As the difference in orientation between $\mathbf{m}_i$ and $\mathbf{m}_j$ becomes larger, we expect a larger torque. In the four-neighbor dot-product representation, however, the exchange energy attributed to $\mathbf{m}_i$ and $\mathbf{m}_j$ is proportional to $\cos(\theta_{ij})$, where θ_{ij} is the angle between $\mathbf{m}_i$ and $\mathbf{m}_j$, and the magnitude of the torque is proportional to $\sin(\theta_{ij})$. The four-neighbor dot product representation describes a torque that actually *decreases* as θ_{ij} becomes greater than $\pi/2$.

1.2 Four-neighbor angle

In this representation, the magnetization interpolation is a uniform rotation between the moments at the two nearest grid points. This interpolation preserves $\mathbf{m} = 1$ in the interpolated region, and the torque required to increase the angle between adjacent spins increases up to $\theta_{ij} = \pi$. The exchange energy is

$$E_{\text{ex,4angle}} = \frac{A}{2}\sum_i \sum_{nn=1}^{4} \theta_{i,nn}^2 \quad (4)$$

and the exchange field is

$$\mathbf{H}_{\text{ex,4angle},i} = \frac{2A}{\mu_0 M}\sum_{nn} \theta_{i,nn}\frac{\mathbf{m}_{nn}}{\sin\theta_{i,nn}}. \quad (5)$$

1.3 Eight-neighbor dot product

In this scheme, the magnetization between the discretization grid points is interpolated from the moments at the four nearest grid points. Inside a cell with moments $\mathbf{M}_{i,j}$, $\mathbf{M}_{i+1,j}$, $\mathbf{M}_{i,j+1}$ and $\mathbf{M}_{i+1,j+1}$ at the four corners, the magnetization $\mathbf{M}(x,y)$ is given by

$$\mathbf{M}(x,y) = \mathbf{M}_{i,j}(1-x)(1-y) + \mathbf{M}_{i+1,j+1}xy + \mathbf{M}_{i,j+1}(1-x)y + \mathbf{M}_{i+1,j}x(1-y), \quad (6)$$

where x and y are in units of the grid spacing. This interpolation allows the magnitude of $\mathbf{m}$ to deviate from a value of 1 within a cell, but it does make the magnetization continuous everywhere. A similar scheme for micromagnetics has been presented for triangular and tetrahedral finite element meshes [1].

Using this interpolation, the gradients appearing in (1) are found from straightforward differentiation of (6). The exchange energy is given by

$$E_{\text{ex,8dot}} = \frac{A}{3}\sum_i \sum_{nnn=1}^{8} (1 - \mathbf{m}_i \cdot \mathbf{m}_{nnn}), \quad (7)$$

where the inner sum is over four nearest neighbors and four next-nearest neighbors, weighted equally. The exchange field is

$$\mathbf{H}_{\text{ex,8dot},i} = \frac{2A}{3\mu_0 M}\sum_{nnn=1}^{8} \mathbf{m}_{nnn}. \quad (8)$$

Table 1: Analytical expressions for E_{ex} for a magnetization spiral evaluated for several representations on a grid with spacing Δ.

Model	E_{ex}
Continuum	Ak^2
4-dot	$\frac{2A}{\Delta^2}[2 - \cos(k_x\Delta) - \cos(k_y\Delta)]$
4-angle	Ak^2; $k\Delta \leq \pi$
8-dot	$\frac{2A}{3\Delta^2}[4 - \cos(k_x\Delta) - \cos(k_y\Delta)$ $- \cos((k_x + k_y)\Delta)$ $- \cos((k_x - k_y)\Delta)]$

2 Comparison of Representations

2.1 Spiral Magnetization

In this section the above discretized expressions for the exchange energy are compared with the continuous expression in (1) for a magnetization configuration where (1) can be evaluated explicitly, namely

$$m_x + im_y = e^{i\mathbf{k}\cdot\mathbf{r}}. \quad (9)$$

Substituting this expression into (1), we find that the exchange energy density—the integrand in (1)—is Ak^2. The discretized expressions (2), (4), and (7), can be evaluated for the magnetization spiral using the following relations:

$$\begin{aligned} \mathbf{m}_i \cdot \mathbf{m}_j &= \cos[\mathbf{k}\cdot(\mathbf{r}_j - \mathbf{r}_i)] \quad &(10a)\\ \theta_{i,j} &= \mathbf{k}\cdot(\mathbf{r}_j - \mathbf{r}_i) \quad &(10b)\end{aligned}$$

Values for the energy density are presented in Table 1. All three discrete representations give $E_{\text{ex}} = Ak^2$ for $k\Delta \ll 1$, where Δ is the grid spacing.

The 4-dot and 8-dot expressions of the exchange energy are anisotropic; for a spiral with a given value of $|\mathbf{k}|$, the exchange energy depends on the direction of $\mathbf{k}$, as illustrated in Fig. 1. We

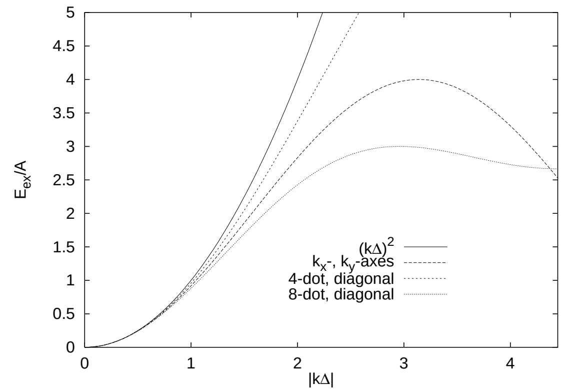

Figure 1: Plots of $E_{\rm ex}$ for wave vectors directed along the k_x or k_y axes and along the grid diagonal, $k_x = k_y$. The 4-dot and 8-dot expressions give identical results for wave vectors parallel to the coordinate axes.

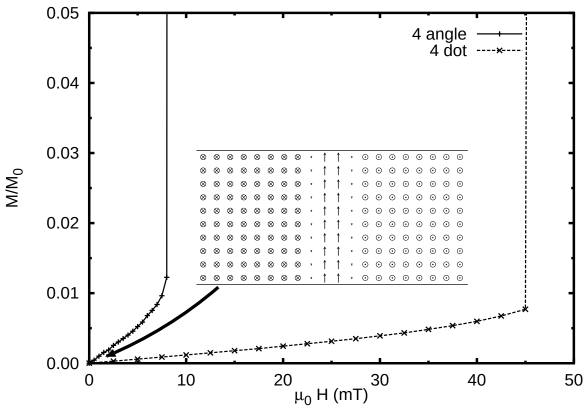

Figure 2: Normalized out-of-plane moment as a function of applied out-of-plane field for 'hcp cobalt' material parameters. Inset: The zero-field magnetization configuration for the 4-angle representation.

note in passing that a dot-product-based expression for the exchange energy with greater symmetry can be constructed by considering expressions of the form

$$E_{\rm ex} = \frac{A}{1+2\beta} \sum_i \left[\sum_{nn}^{4} (1 - \mathbf{m}_i \cdot \mathbf{m}_{nn}) + \beta \sum_{nnn}^{4} (1 - \mathbf{m}_i \cdot \mathbf{m}_{nnn}) \right]. \quad (11)$$

Using the relations in (10) and expanding to $O(k\Delta)^4$, the maximum symmetry is obtained when the resulting expression depends only on powers of $(k_x^2 + k_y^2)$, with terms proportional to powers of $k_x k_y$ set equal to zero. This condition is satisfied when $\beta = 1/4$.

2.2 Domain wall mobility

We also compared the effects of the exchange energy representation on the critical field needed to move domain walls. To isolate the effects of the choice of exchange energy representation, the magnetostatic fields have been neglected. Values of $A = 1.3 \times 10^{-11}$ J/m, $K_{\rm u} = 5.3 \times 10^5$ J/m^3 and $M_{\rm s} = 1.45 \times 10^6$ A/m corresponding to 'hcp cobalt' were used.

Virgin curves for a 200x50 nm section of hcp cobalt with $\Delta = 5$ nm are presented in Fig. 2. Because the domain wall lies parallel to an axis of the grid, the 4-dot and 8-dot representations are identical. In addition, with zero magnetostatic field, the problem becomes essentially one-dimensional. The critical field for the 4-angle is less that that for the 4-dot representation. This effect is associated with the fact that the 4-angle exchange and the dot-product exchange representations have very different behavior when the angles between adjacent spins are large.

The critical fields for domain wall motion using the 'hcp cobalt' parameters are plotted in Fig. 3 as a function of cell size. The critical field drops to zero when the cell size is approximately equal to the exchange length, $\delta = (A/K_{\rm u})^{1/2} \approx 5.0$ nm.

2.3 Vortex Mobility

We next compare the properties of these representations using a vortex magnetization configu-

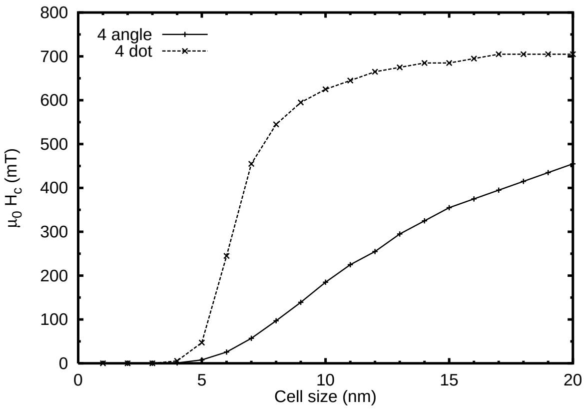

Figure 3: Critical field for wall motion as a function of cell size for 'hcp cobalt' material parameters.

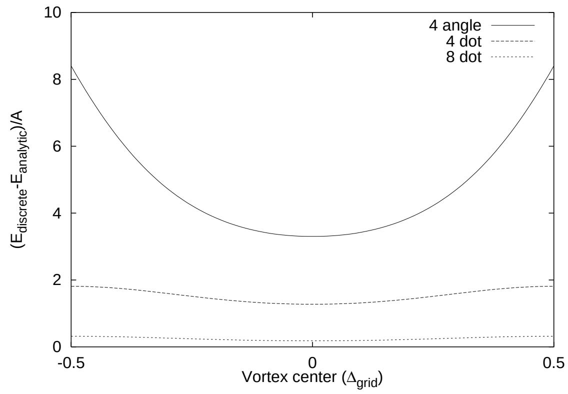

Figure 4: Exchange energy as a function of the vortex center position within a cell for three representations of the exchange energy.

ration. Vortices are often present in micromagnetic models of thin films [2, 9, 11, 10, 12]. Because of the translation invariance of an infinite, uniform thin film, the exchange energy of a magnetic vortex should not depend on the position of the vortex. The discretization of the film into a grid breaks the translation invariance, raising the possibility of vortex pinning as an artifact of the grid. We have evaluated the exchange energy of a vortex as a function of the location of the vortex center for the three exchange energy representations described above.

In a continuous medium, the exchange energy of a pure 2-D vortex is not well defined. The integral in (1) diverges logarithmically both at the center of the vortex and at large distances from the center. The discretized expressions for the exchange energy of the vortex do not diverge at the center of the vortex, but they also diverge at large distances. To circumvent these problems, we limit our continuous medium calculation to a ring-shaped region with an inner radius of $\Delta/3$ and an outer radius on the order of 100Δ. The discretized calculations are limited to the same outer radius, with no inner radius limit. (At large radii the discretized calculations converge rapidly enough to the continuous (analytic) calculations so that increasing the outer radius beyond 100Δ does not significantly change $E_{\rm discrete} - E_{\rm analytic}$.) The results are depicted in Fig. 4. In all 3 cases the minimum energy configuration occurs when the vortex center is in the middle of a cell, i.e., away from the discretization grid points. The effect is largest for the 4-angle exchange formulation.

In the energy well calculation described in the previous paragraphs, the spin directions were determined solely by their position relative to the vortex center, not by energy minimization. To examine how grid pinning of vortices affects actual micromagnetic calculations, we calculated the field needed to move a vortex from the center of a 1 μm square of 'permalloy'. Because similar grid pinning effects may exist in the calculation of demagnetizing fields, we isolated the effects of the exchange energy representation by replacing the dipole–dipole fields with a uniaxial, easy plane anisotropy, $K_{\rm u} = \frac{1}{2}\mu_0 M_{\rm s}^2 = 4 \times 10^5$ J/m^2. The other parameters used in this calculation are $M_{\rm s} = 8.0 \times 10^5$ A/m, Δ = 50 nm, and $A = 1.3 \times 10^{-11}$ J/m. The results are plotted in Fig. 5.

The 4-angle representation of the exchange

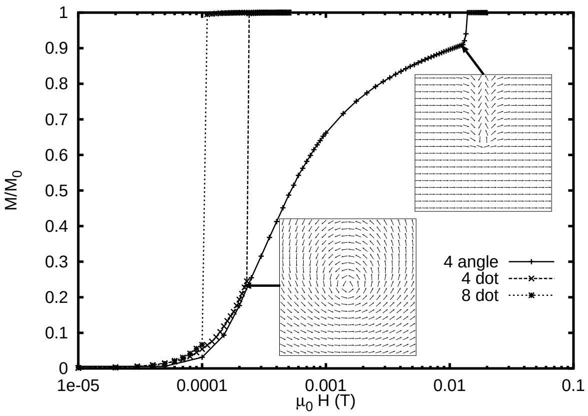

Figure 5: Virgin curves for 1 μm $\times$ 1 μm 'permalloy' squares calculated from an initial state containing a vortex at the center using three representations of the exchange energy. Δ = 50 nm.

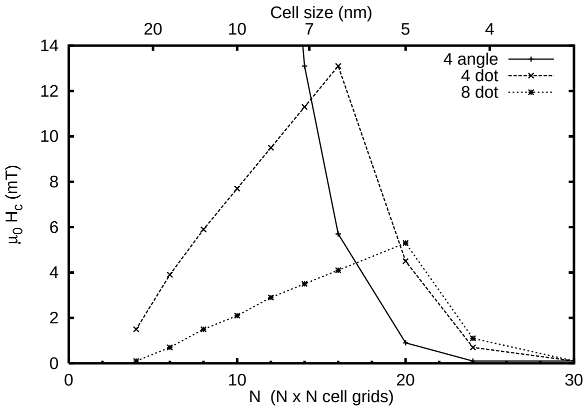

Figure 6: Field required to move initially centered vortices in 100 nm 'permalloy' squares on an $N \times N$ grid as a function of N. The maximum value for $\mu_0 H_{\mathrm{c,4angle}}$ is about 75 mT, occurring at $N = 8$.

energy, which gives the most accurate results for calculation of magnetization spirals, is found to produce undesirably strong grid pinning of vortices. This effect is amplified in Fig. 5 by the fact that the outer portions of the vortex structure collapse before the vortex core moves, reducing the effective interaction of the vortex with the applied field.

As a function of cell size, one might initially expect that smaller cell sizes would reduce the effects of discretization. However, cell size reduction reduces the width of the wells depicted in Fig. 4 without changing their depth, increasing the steepness of the well sides. The field required to move initially centered vortices in 100 nm squares of 'permalloy' is given in Fig. 6 as a function of N, where the squares are discretized onto an $N \times N$ grid. Demagnetization fields are replaced by a uniaxial anisotropy, as above.

As the cell size is decreased (increasing N), the critical field initially increases linearly with N, in agreement with increased pinning due to steepening of the sides of vortex energy wells. When the cell size decreases to a size on the order of the exchange length, $\delta = (A/K_{\mathrm{u}})^{1/2} \approx 5.7$ nm, $N \approx 18$, the critical field begins to decrease. Concurrent with this decrease, the vortex develops an out-of-plane moment in the vortex core. As the mesh becomes fine enough to model the internal structure of the vortex, further refinement reduces the critical field for vortex mobility to zero.

3 Conclusions

We have compared the characteristics of three representations of the exchange energy for a 2-D square grid, using comparison with continuum results and tests of vortex and domain wall mobility. For a magnetization spiral, we find the following points:

- all three representations give accurate results for $k\Delta \ll 1$,
- the 4-angle representation gives the most accurate evaluation of the exchange energy for $k\Delta \leq \pi$, and

- the dot-product representations are notably anisotropic for $k\Delta > 1$.

The domain wall and vortex mobility studies show the following:

- grid-induced energy wells for vortices and domain walls can be significant,
- domain walls and vortices are pinned when the grid size is too large,
- the 4-angle representation produces the largest vortex pinning, and the least domain wall pinning,
- the pinning strength for domain walls and vortices drop as the grid size becomes smaller than the relevant exchange length, so that the vortex core and domain wall structure are resolved.

References

[1] W. Chen, D. R. Fredkin and T. R. Koehler, IEEE Trans. MAG 29 (1993) 2124.

[2] S. W. Yuan, H. N. Bertram, J. F. Smyth and S. Schultz, IEEE Trans. MAG 28 (1992) 3171.

[3] Z. Guo and E. Della Torre, J. Appl. Phys. 75 (1994) 6770.

[4] A. E. LaBonte, J. Appl. Phys. 40 (1969) 2450.

[5] A. Aharoni and J. P. Jakubovics, IEEE Trans. MAG 29 (1993) 2527.

[6] W. Williams and D. J. Dunlop, Nature 337 (1989) 634.

[7] M. R. Scheinfein, J. Unguris, J. L. Blue, K. J. Coakley, D. T. Pierce, R. J. Celotta, and P. J. Ryan, Phys. Rev. B 43 (1991) 3395.

[8] S. Müller-Pfeiffer, M. Schneider, and W. Zinn, Phys. Rev. B. 49 (1994) 15745.

[9] J. O. Oti, IEEE Trans. MAG 29 (1993) 1265.

[10] T. R. Koehler and D. R. Fredkin, IEEE Trans. MAG 28 (1992) 1239, D. R. Fredkin and T. R. Koehler, J. Appl. Phys. 67 (1990) 5544.

[11] J.-G. Zhu and H. N. Bertram, J. Appl. Phys 63 (1988) 3248.

[12] J. Gadbois and J.-G. Zhu, IEEE Trans. MAG 31 (1995) 3802.